ORIGINAL ARTICLE

Biochemical changes in the cytoplasm of bovine oocytes during the *in vitro* maturation process: a Raman microscopy study

Luis Emanuel Jimenez[1] · Ana Carolina Juárez[1,2] · Mariela Roldán-Olarte[3,4] · Rosa María Susana Álvarez[1,2]

Abstract

The sequence and chronology of the main biochemical changes occurring in the cytoplasm of bovine oocytes during the *in vitro* maturation process were tracked by Raman microscopy applied to cells previously subjected to enzymatic digestion of the zona pellucida. Specific spectral markers for proteins, lipids and carbohydrates were used to evaluate the developmental status of the ooplasm at four different times. Spectral changes revealed that lipid accumulation was dominant during the first six hours of culture while protein content reached the average levels characteristic of mature oocytes within the last four hours of the maturation process. A time-dependent decrease in carbohydrates was also observed. Finally, the carbohydrate-to-protein (P_{1037}/P_{1002}) ratio proved to be sensitive enough to determine the cytoplasmic maturation state of bovine oocytes and promises to be useful in future research aimed at optimizing culture conditions through the promotion of protein accumulation in the ooplasm.

Keywords Bovine ooplasm · Lipids · Macromolecules · Proteins

Introduction

The biotechnology of animal reproduction aims at improving the reproductive efficiency of livestock species of interest, especially in countries with an economy based on mixed crop-livestock systems. With this purpose in mind, several studies have focused on the optimization of *in vitro* embryo production (IVP) of farm animals, cattle among them. IVP has three main stages: *in vitro* maturation (IVM) of the cumulus-oocyte complexes (COC), *in vitro* fertilization (IVF) of matured oocytes, and *in vitro* culture (IVC) of embryos in a synthetic medium. The IVP of bovine embryos has limitations with respect to blastocyst yield and embryo quality. The low yield of IVP has been attributed to the lower developmental competence of *in vitro* matured oocytes compared to *in vivo* matured ones (Lonergan and Fair 2016; Rizos et al. 2002). Therefore, IVM is undoubtedly a crucial stage that directly affects IVP; consequently, the improvement in maturation conditions to promote an increase in fertilization and embryo development rates is of vital importance (Lonergan and Fair 2016; Ward et al. 2002). The maturation stage of the oocyte is determined by essential biochemical and morphological changes undergone by the cell during its growth and development. These alterations can be separated into two different but synchronized events called nuclear and cytoplasmic maturation. At the beginning of nuclear maturation, chromosomes remain decondensed in the nucleus, during what is known as the germinal vesicle (GV) stage; when the first meiotic division starts, chromosomes initiate condensation and the germinal vesicle envelope breaks down (GVBD); after that, the first metaphase (MI) is formed in which the first polar body is released; finally, the oocyte remains arrested in metaphase II (MII) until fertilization occurs (Kruip et al. 1983; Sirard et al. 1989). During cytoplasmic maturation, the process involves the increase in the number of organelles, mainly mitochondria, cortical granules and their reorganization, as

✉ Rosa María Susana Álvarez
  maria.alvarez@fbqf.unt.edu.ar

[1] Instituto de Química del Noroeste Argentino (INQUINOA), CONICET-UNT, Tucumán, Argentina

[2] Facultad de Bioquímica, Química y Farmacia, UNT, Instituto de Química Física, San Lorenzo 456, San Miguel de Tucumán, T4000CAN Tucumán, Argentina

[3] Instituto Superior de Investigaciones Biológicas (INSIBIO), CONICET-UNT, Tucumán, Argentina

[4] Instituto de Biología 'Dr. Francisco D. Barbieri', Facultad de Bioquímica, Química y Farmacia, UNT, Chacabuco 461, San Miguel de Tucumán, T4000ILI Tucumán, Argentina

well as the accumulation of mRNA, proteins and lipids. All these necessary modifications must occur in an orchestrated and balanced manner to reach the mature state of the cell, and also to insure both successful fertilization and subsequent early embryonic development (Ferreira et al. 2009; Niimura et al. 2002).

In recent years, Raman microscopy has become a powerful tool for the analysis of biological samples since it provides valuable information about the biochemical and structural composition of cells quickly and without interference from surrounding water molecules (Bonnier and Byrne 2012; Bogliolo et al. 2020). In particular, this technique has been used in several studies of the female gametes of small mammalians such as mouse and cat, focusing on the characterization of the zona pellucida (ZP) and the cytoplasm. For instance, Davidson et al. (2013), by comparing the Raman spectral profiles of the cytoplasm of *in vitro* mature mouse oocytes with *in vivo* mature ones, demonstrated that cells treated under *in vitro* conditions were protein deficient. More recently, three-dimensional molecular Raman images of living oocytes allowed the detection of small variations in protein, lipid and nucleic acid bands between cells at different maturation stages (GV, MI and MII) (Heraud et al. 2017). Ishigaki et al. (2019) monitored the bands attributed to phosphoric acid in the cytoplasm of *in vivo* matured mouse oocytes at different times and concluded that these features might act as potential biomarkers of cell competence and development. Okotrub et al. (2018) observed the changes in the intensities of the lipid bands that occurred in cat oocytes during their freezing and thawing in order to provide information on the effects of cryopreservation methods. Conversely, only a few research works used Raman spectroscopy in the study of oocytes from larger mammals such as ovine and bovine species. In this connexion, the Raman studies on the ZP and the cortex of the ovine oocytes after their cryopreservation carried out by Bogliolo et al. (2012, 2014) are worth mentioning. In these research works, the spectra showed modifications in the secondary structure of the proteins and in the carbohydrate residues of both cell regions but, according to the spectral maps, the cortex experienced changes mainly in the protein content (Bogliolo et al. 2012, 2014). As to the bovine species, Rusciano et al. (2017) evaluated the changes in the ZP and cytoplasm of vitrified/warmed *in vitro* matured oocytes at different post-warming times and observed a decrease in the content of unsaturated lipids, while the proteins showed alterations in their secondary structure. Our group has also contributed to a better understanding of the biochemical and structural changes that occur in bovine oocytes upon the *in vitro* maturation process by using Raman microscopy. In a preliminary study, we carried out a detailed analysis of the spectral changes undergone by the bands of the ZP glycoproteins. We observed a marked decrease in the intensity of sugar

Raman bands and intensifications in those corresponding to proteins in the spectra of mature oocytes, which were indicative of a structural reorganization of the ZP consisting in a greater exposure of the terminal sugar residues (e.g., sialic acid) while the glucan nucleus was masked by the polypeptide chain (Rizo et al. 2016). Recently, we characterized the immature and *in vitro* mature states of the bovine ooplasm using specific bands of lipid, protein, and carbohydrate vibrations; oocytes were previously subjected to enzymatic digestion of their ZP to prevent interferences (Jimenez et al. 2019). The spectra of mature oocytes showed a marked increase in both lipid and protein content while sugars decreased considerably compared to the immature oocytes (Jimenez et al. 2019).

On the basis of our previous results, the aim of this work was to carry out a more in-depth investigation of the biochemical changes that occur in the cytoplasm of bovine oocytes during IVM to determine their sequence/chronology and to evaluate the global changes in the content of the main bio-components by using Raman microscopy. To this end, the spectra of oocytes obtained at intermediate stages of IVM (*in vitro* cultured for 6 or 18 hours) were compared with the spectra of control samples for immature and *in vitro* matured oocytes.

At present there is great interest in improving the IVM media in order to ensure a) the developmental competence of bovine oocytes and increase the blastocyst rate and b) the obtainment of good quality embryos to transfer them to a recipient female. In this context, the results presented here provide valuable knowledge for further studies on the spectral characteristics of oocytes undergoing maturation in supplemented media with specific components. Detection by Raman microscopy of improvements or impairments in oocytes subjected to IVM, prior to IVF or embryo culture, would substantially reduce losses in embryo production.

Materials and methods

Cumulus oocytes complexes collection

Bovine ovaries were collected from heifers (*Bos taurus*) at a local abattoir and transported in sodium phosphate buffer (PBS), pH 7.4, at 25-30 °C for processing within 2 h after collection. For the present study, 20 ovaries from 10 heifers were employed. Cumulus oocytes complexes (COCs) were obtained by aspiration from follicles of 2 to 8 mm in diameter with an 18-gauge needle connected to a 5 mL disposable syringe containing ~1 mL of Tirodes Albumin Lactate Piruvate medium (TALP) supplemented with 10 mM N-2-hydroxyethylpiperazine-Ń-2-ethane-sulfonic acid (HEPES, Genbiotech, Argentina) plus 10% (v/v) fetal bovine serum (FBS, Internegocios, Argentina). Eighty immature

COCs (*n*=80), with uniform ooplasm and intact and compact cumulus cell layers, were selected by using a stereoscopic microscope (Olympus SZ51). After two washes in TALP–HEPES medium, COCs were randomly distributed into two groups. In the first group, COCs that remained in the immature state were separated and reserved for nuclear staining test and Raman measurements, described later on in this work (n=20); they were called immature COCs. The second group of COCs (*n*=60) underwent an *in vitro* maturation process.

In vitro maturation

In vitro maturation (IVM) of bovine COCs was carried out as described previously (García et al. 2015a). COCs destined for maturation were divided into three groups with *n*=20 complexes each. These were transferred to 100 μL droplets of *in vitro* maturation medium containing tissue culture medium (TCM) -199 (Gibco, USA). This medium was supplemented with 10% (v/v) FBS, 0.375 IU mL-1 human follicular stimulant hormone plus luteal hormone (HMG Ferring ®, Argentina), 0.13 mmol L-1 of sodium pyruvate (Sigma P4562, USA), 20 mM cysteamine (Sigma M9768, USA), and 1% antibiotic–antimycotic solution (Gibco, USA). Each drop of the medium contained a maximum of 10 COCs. Each of the three groups was maintained in IVM conditions (culture medium at 38.5 °C and under CO_2 at 5% atmosphere) for 6, 18, or 22 hours; 22 hours is the time required to complete the IVM protocol used here (García et al. 2015b). These maturation times were selected to determine the general characteristics of the cytoplasm, evaluated in terms of the relative abundances of the main bio-components, and so relate what happened in the cytoplasm with what happened in the nucleus: before starting the maturation process (t= 0h), the oocyte presents an intact nucleus surrounded by the nuclear envelope (GV stage); after 3 to 6 hours of development, chromosomes condensation and fragmentation of the nuclear envelope (GVBD stage) begins; between 12-18 hours of culture, the oocyte is characterized by the formation of the meiotic spindle (MI stage) and finally, after 19 to 22 hours, the first polar body is released and the oocyte reaches the stage of metaphase II (MII) (Kruip et al. 1983; Sirard et al. 1989).

Evaluation of cumulus expansion

Cumulus expansion was evaluated by recording digital images with a stereomicroscope (Olympus SZ51) with a magnification of 25X. Each of the three groups of cultured COCs as well as the group of immature COCs were assessed. The cumulus area from each oocyte was measured with a computerized image-digitizing system (ImageJ software) which allows the measurement of irregular areas. The relation between each cultured COC area for a specific time period and that of immature COC were determined (Rizo et al. 2021).

Preparation of oocytes for the different analyses

The cumulus cells of the four different COCs groups were removed by pipetting in warm TALP–HEPES medium with 0.3 mg mL-1 hyaluronidase (Sigma Aldrich, USA) as previously described (García et al. 2015a) . Oocytes were washed three times with PBS containing 1% bovine serum albumin (BSA, DSF Lab, Argentina). After that, the four groups of oocytes without cumulus cells were divided into two subgroups each. In one of the respective sub-groups, the oocytes with their intact ZP were fixed for 30 minutes in 4% paraformaldehyde solution (w / v), (Rizo et al. 2021; Jimenez et al. 2019; Rusciano et al. 2017), washed three times in PBS/BSA and stored at 4 °C to evaluate their nuclear maturation with a staining technique. In the remaining subgroups, the oocytes were treated with 0.4% (w / v) pronase (*Steptomyces griseus* protease, Sigma, USA) to completely digest the ZP. The zona-free oocytes, all of them presenting a visually homogeneous ooplasm, were washed in PBS/BSA three times, fixed for 30 minutes in 4% paraformaldehyde solution (w / v), washed three times in PBS/BSA and stored at 4 °C for Raman measurements. For spectral analysis, the four sample collections were named 0H, 6H, 18H and 22H, according to the culture time to which they were subjected. Samples named as 0H and 22H were considered immature and mature control groups, respectively.

For clarity, Fig. 1 shows a summary of the experimental design, which ranges from the aspiration of the COCs to the time when oocytes were ready for Raman measurements. The whole experimental procedure was performed in duplicate carried out in different experiments.

Nuclear maturation controls

In order to support the results derived from the vibrational analyses, the nuclear maturation stages of the oocytes belonging to the four sub-groups of cells were determined by the nuclear staining technique and subsequent observation by epifluorescence microscopy. Assays were performed by following a protocol previously described (Roldán-Olarte et al. 2017). Briefly, for each sample group and experiment, the chromatin of 20 oocytes was stained with 1 μg / mL of Hoëchst 33342 (Sigma Aldrich, USA) for 15 minutes, then washed and mounted on 2 μL of mounting medium (50% (v / v) PBS, 50% (v / v) glycerol, 0.0025 μg / mL Hoëchst). Finally, the oocytes were placed between a coverslip and a glass slide and sealed with nail polish. Slides were examined by using an epifluorescence microscope (Olympus BX40). Oocytes that showed a well-defined nucleus (GV), GVBD,

Fig. 1 **A** Schematic representation of the experimental design of this study. **B** Image of the cytoplasm of a zona-free oocyte cultured *in vitro* for 6 hours, obtained with a confocal Raman microscope using a 20X objective. The numbers indicate the approximate locations of the sampling points used for data collection
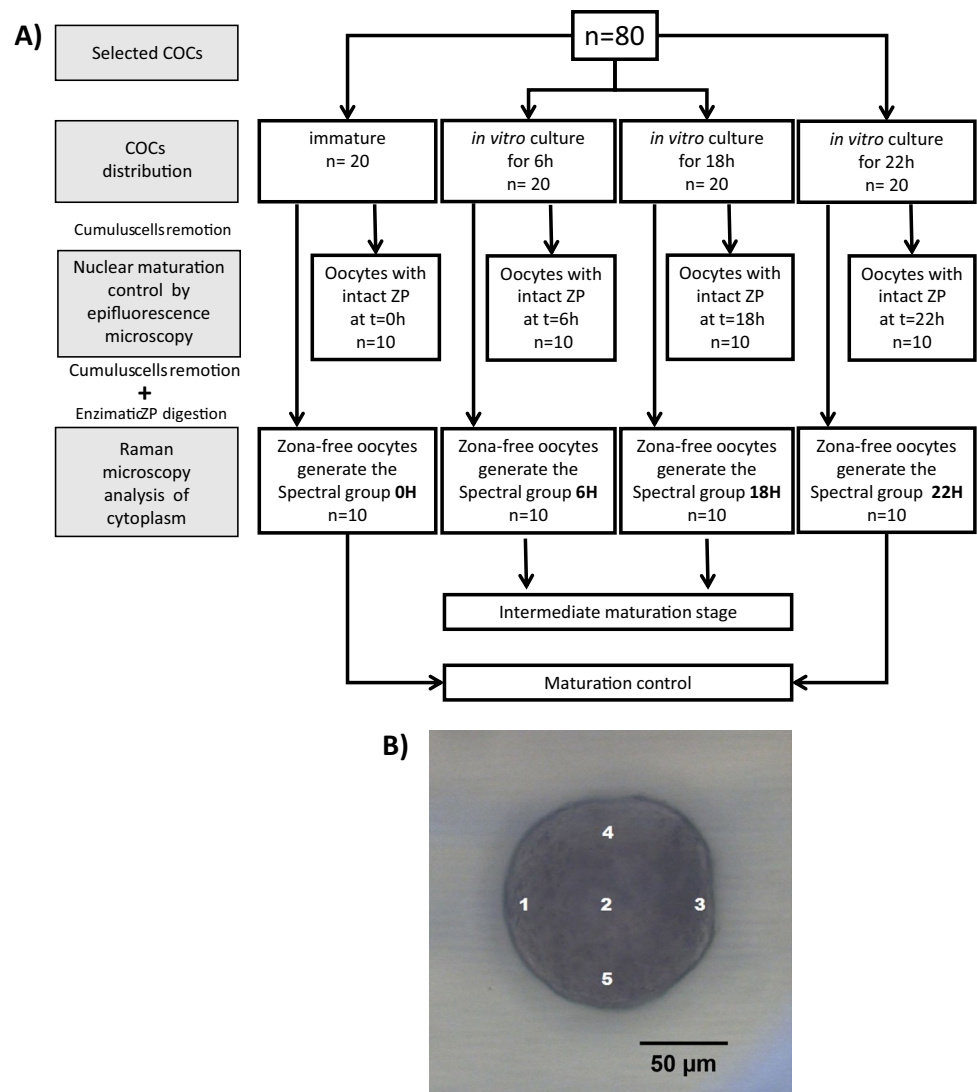
or a visible first metaphase plate (MI), were considered as immature, while those that showed the presence of the first polar body or the second metaphase plate (MII), were considered mature oocytes (Ferreira et al. 2009).

Raman microscopy measurements

Raman measurements were obtained from ZP-free oocytes from the four groups formed here. Since some cells were partially damaged during ZP removal, the total number of oocytes suitable for analysis by Raman microscopy varied in the groups: 0H (*n*=14), 6H (*n*=13), 18H (*n*=17), and 22H (*n*=14), belonging to two experiments (the original and the duplicate, detailed above). The oocytes were individually transferred to a gold-coated slide, suitable for Raman microscopy, in 5 µL drops of PBS. Raman measurements, between 3500 and 50 cm^{-1}, were performed with a DXR confocal Raman Microscope (Thermo Fisher Scientific, USA) equipped with a motorized stage with a spatial resolution of 3 µm (x, y axes) and a confocal depth resolution of 2 µm. A diode-pump solid state laser of 780 nm (5 cm^{-1} spectral resolution) was used. For data collection, excitation at 24 mW of power and a confocal aperture of 50 µm slit were used. Samples were focused with a 20X objective. In addition to the excess of PBS medium used during Raman measurements, dehydration of the oocytes caused by long periods of irradiation was prevented and the good condition of the sample was preserved by collecting spectra from a maximum of five sampling points for each oocyte (Jimenez et al. 2019; Rizo et al. 2016). The sampling points were chosen at random but following a previously established order so as to cover the peripheral and central regions of the outermost layers of each oocyte, as indicated in Fig. 1B. Each sampling point yielded one individual spectrum, which was acquired by accumulating 40 expositions with an exposure time of 3 seconds each. All the spectra of a given oocyte were compared among them and those showing a poor signal-to-noise ratio or an excessive contribution from the PBS medium

were rejected; thus, in some cases, the number of individual spectra per oocyte was reduced to four or three. The Raman spectrum of the PBS medium was also acquired to be used as a reference. All spectroscopic experiments were carried out at room temperature.

Data analysis and statistics

Spectral data were processed with the OMNIC 8 Software suite (Thermo Scientific, USA). The total number of collected spectra per group was 62 from 0H, 67 from 6H, 82 from 18H and 66 from 22H. In order to ensure that the PBS medium did not interfere with the observation of the cytoplasm, its spectral contribution was eliminated by subtraction of the PBS spectrum from each cytoplasm spectrum. The resulting spectra were consistent with both the reduction of the band at 1616 cm^{-1} and the flatting of the spectral profile in the 3300-3050 cm^{-1} region, both attributed to the PBS medium (Jimenez et al. 2019; Rizo et al. 2016). Subsequently, all the spectra were individually baseline corrected using a linear algorithm and then smoothed with 13 data point with the Savitzky-Golay algorithm (Savitzky and Golay 1964).

Due to the inhomogeneous distribution of organelles and lipid droplets, especially in the outermost layers of the cytoplasm, spectral differences among the processed spectra belonging to a single oocyte were later averaged to yield a single average spectrum per cell. Then, since the average spectra of the oocytes that were cultured *in vitro* for the same period of time did not show significant differences among them, a single representative spectrum of each group was generated. Four different representative spectra were obtained by taking the arithmetic mean of the 14, 13, 17 and 14 mean spectra corresponding to groups 0H, 6H, 18H and 22H, respectively. The spectra were consecutively compared with each other.

Arithmetic decomposition of the complex spectral region comprised between ~1600 and ~1700 cm^{-1} was performed with the GRAMS/32 software (Thermo Scientific, USA). The number of components in each peak and their locations were first determined by calculating the second derivatives of the representative spectra. The best-fitting procedure, based on the Levenberg-Marquardt method, was applied by using Voight functions (Marquardt 1963); the four parameters (position, height, Gaussian width, and Lorentzian width) were set free while the number of peaks underlying the original curve was fixed; iterations were allowed until solution converged and the best fit was visually evaluated by superimposing the reconstituted curves on the original spectra and by taking into account the maximum proximity between the position of the deconvolved bands and the location of the peaks in the second derivative (Jimenez et al. 2019).

Statistical analyses were performed by considering the 58 average spectra generated in this study. The INFOSTAT software package 2013 (FCA-UNC, Argentina) was used to carry out the Student´s t-test, with significance set at $p < 0.01$, as well as to perform a Principal Component Analysis (PCA) and the receiver operating characteristic (ROC) analysis. The second derivative of all the average spectra in each group were used in statistics based on its well-known usefulness to reveal the fine structure of the bands (Bogliolo et al. 2013, 2014; Jimenez et al. 2019; Wood et al. 2008). Student´s t-test and PCA were applied to the intensities of the characteristic peaks of lipids (at 1300 and 1062 cm^{-1}), sugars (1037 cm^{-1}), and proteins (1340 and 1003 cm^{-1}), extracted from the second derivative of the spectra. It had been previously determined that these signals show a statistically significant variation between immature stages and mature bovine oocytes (Jimenez et al. 2019). The Student's t test propitiated a better comparison between two spectral groups of consecutive cultivation periods by estimating the mean intensity and the variation of the selected peaks. PCA allowed determining the major trends within a given spectral data set based on the principal components PC1 and PC2; these new variables condense the spectral information supplied by such specific peaks. The ROC analysis, limited to monitoring the relative intensities between a lipid or protein peak with regard to the sugar peak, allowed the detection of differences in the content of the major bio-components within the same maturational group.

Results

Cumulus-oocyte-complexes observation

The first morphological indicator that the maturation process is being carried out is the expansion of the cumulus cells mass that surrounds the oocyte. The progressive increase in the size of these cells was evaluated prior to the spectral and staining assays. In the case of COCs grown for 6 and 18 hours, the enlargement was about 30% and 298%, respectively, compared to immature COCs, while for COCs that were kept for 22 hours in the culture medium, the expansion was 419%. These results confirmed the progress of IVM over time.

Nuclear maturation rate of bovine oocytes

The progress of IVM was additionally monitored by evaluating the degree of nuclear maturation at each time point assayed by staining the oocytes with Hoëscht 33342 to observe the nuclear morphology.

As expected, all the oocytes in the 0H group were effectively identified as immature since the nuclei were in the GV stage, while 73.7% of oocytes cultured for 22 hours were in the MII stage. The fluorescence-based technique also determined that 75% of oocytes cultured for 6 hours remained in

the GV stage while the rest moved on to GVDB. The group of oocytes subjected to maturation for 18 hours resulted in two subgroups: 50% of oocytes with immature nucleus (31% of oocytes were in the MI stage and the rest in GV or GVBD) and 50% in the MII stage, that is, oocytes with nuclear maturation.

Fig. 2 Representative Raman spectra of the four groups of oocytes generated in this study, truncated to the region comprised between 3100 and 2800 cm^{-1}. The peaks associated with the $\nu_s CH_3$, $\nu_{as} CH_2$, and $\nu_s CH_2$ modes are highlighted
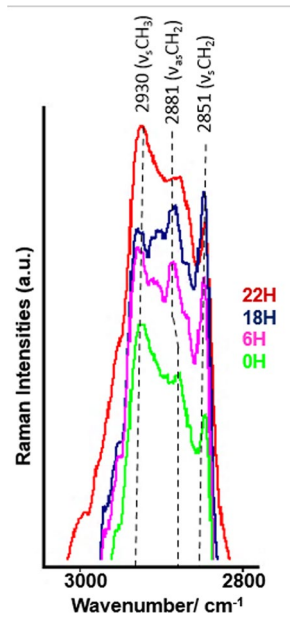
Raman spectroscopy analysis

The Raman spectral analysis of ooplasms at two intermediate maturational stages (6H and 18H groups) was carried out by comparison both between their representative spectra and with those in the control groups (0H and 22H groups).

The identification and comparative analysis of the specific vibrational modes of the proteins, lipids, and carbohydrates, here considered as the relevant components, allowed us to infer the main biochemical alterations that the cell underwent at the selected times of the maturation process.

Figure 2 shows the spectral region comprised between 3100 and 2800 cm^{-1} extracted from the representative spectra belonging to the four groups of zona-free oocytes here generated. This region is characterized by the presence of the strongest Raman bands of the spectra, originated by the superposition of various C-H stretching modes corresponding to the CH$_2$ and CH$_3$ groups of all the macromolecules of the cytoplasm. Similarly, Fig. 3 compares the 1800-900 cm^{-1} spectral region obtained for the four groups. Positions, relative intensities, and shapes of most of the signals appearing in this sub-region of the fingerprint have already been well determined for mammalian oocytes (Heraud et al. 2017; Ishigaki et al. 2019; Jimenez et al. 2019; Okotrub et al. 2018). Conversely, the spectral region below 900 cm^{-1} is normally excluded from the vibrational study of biological systems due to the inherent poor signal-to-noise ratio

Fig. 3 Representative Raman spectra of the four groups of oocytes generated in this study, truncated to the region comprised between 1800 and 900 cm^{-1}. The spectra were normalized with the band at 1441 cm^{-1} ($\delta CH_3/CH_2$) for better comparison. The grey areas indicate the location of the protein vibrational modes. Lipid bands are highlighted with *. Carbohydrate bands are highlighted with **. The vertical lines show the most relevant bands arising from this analysis. Included wavenumbers for specific vibrations correspond to the bands used for statistics. Ar: vibration of aromatic amino acids
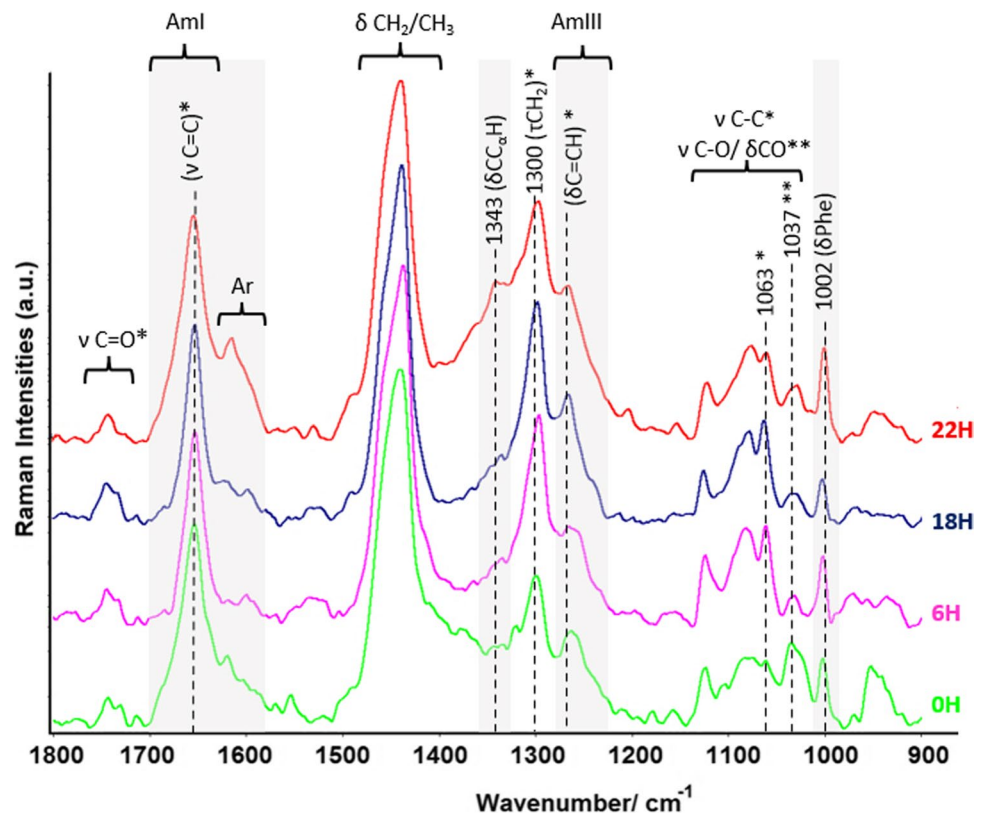
that makes band assignments difficult (Davidson et al. 2013; Krafft et al. 2005; Wood et al. 2008). Table 1 lists most of the bands observed in the 3000-900 cm^{-1} region of the representative spectrum of each group of oocytes together with the proposed assignment and the references.

The tracking of the main biochemical changes that occurred in the cytoplasm of bovine oocytes as the *in vitro* maturation progressed was performed by comparing two consecutive culture periods.

0H spectrum vs 6H spectrum

The spectral profile corresponding to the C-H stretching bands was significantly different in the 6H group with respect to the one obtained from immature oocytes (see Fig. 2): the relative intensities of the bands at 2851 cm^{-1} (ν_sCH_2) and 2930 cm^{-1} (ν_sCH_3) were visibly altered while the $\nu_{as}CH_2$ feature shifted from 2881 cm^{-1} (in 0H) to 2888 cm^{-1} (in 6H). The $I\nu_sCH_2/I\nu_sCH_3$ ratio was proposed to infer the relative abundances between lipids and proteins in the ooplasm (Czamara et al. 2017; Krafft et al. 2005;). The increment of about 21% in the intensity ratio in the 6H spectrum was then indicative of an enhanced lipid content upon six hours of culturing. In turn, the upshift of the $\nu_{as}CH_2$ band was associated with a higher proportion of unsaturated lipid chains. The peak at ~2883 cm^{-1} was assigned to lipids and triglycerides with saturated acyl chains, and the signal at ~2895 cm^{-1} to systems containing double bonds in their chains (Czamara et al. 2014, 2017; Lee and Bain 2005; Sosa Morales et al. 2015, 2019).

When comparing the region between 1800-900 cm^{-1} of both spectra, one of the most remarkable differences was the enhancement on the band centered at 1300 cm^{-1} (τCH_2 mode of lipid acyl chains) in the 6H group. In addition, the drastic changes in both the relative intensity and the shape adopted by the complex contour, observed in the region between 1060 and 1130 cm^{-1}, were produced by the presence of various vibrational modes of both lipids and carbohydrates (see Fig. 3, Table 1). This resulted in a band cluster similar to the one typically observed for the fluid phase of pure lipid systems: a central band at 1084 cm^{-1} (associated with methylene groups in *gauche* conformation, $\nu(C-C)_G$) and the flanking bands located at 1125 and 1063 cm^{-1} (associated with the alkyl chains in trans conformations, $\nu_s(C-C)_T$ and $\nu_{as}(C-C)_T$, respectively). Then, the band at 1104 cm^{-1} (in 0H spectrum), which was associated with a sugar $\nu C-O/\delta C-O-H$ mode, was completely eclipsed in the 6H spectrum. On the other hand, the band centered at 1655 cm^{-1} was observed to be narrower and cleaner at its base than in the 0H; this feature receives contributions from the amide I (AmI) mode of the different secondary structure domains of proteins and of N-acetylated carbohydrates as well as from the stretching of unsaturated lipid chains ($\nu C=C$) (Jimenez et al. 2019; Lee

and Bain 2005; Rygula et al. 2013). Better insights of this composite band were obtained upon deconvolution and peak fitting procedures; this was applied to the four representative spectra generated in this study and shown in Fig. 4. In this way, it was clearly observed that the component at 1655 cm^{-1} in the 6H spectrum (see Fig. 4b), assigned to the lipid $\nu C=C$ vibration, stood out over all the others, while the component associated with the AmI mode of acetylated sugars (1640 cm^{-1}) evidenced a significantly lower contribution than in the 0H spectrum (Fig. 4a). Additional evidence of the decrease in sugar contribution to the spectrum of oocytes cultured for six hours was given by the weakness of the feature at 1037 cm^{-1} (assigned to a $\nu C-O/\delta C-O-H$ mode, see Fig. 3).

6H spectrum vs 18H spectrum

The most noticeable change observed in the spectrum of oocytes cultured for 18 hours compared to the spectrum of those treated for six hours is the great enhancement shown by the C-H stretching bands of the methylene groups (see Fig. 2). The $I\nu_sCH_2/I\nu_sCH_3$ intensity ratio was ~17% higher than in the 6H spectrum, which indicated an increased predominance of the total lipid content over the protein content in oocytes subjected to *in vitro* culture for 18 hours.

The remaining lipid bands appearing in the fingerprint region of the 18H spectrum (Fig. 3) also evidenced enhancements, albeit of lower magnitude, with the exception of a neat spectral difference detected with the naked eye in the 1250-1280 cm^{-1} region. The broad and structured band observed both in the spectra of immature oocytes and in that of oocytes cultured for six hours, assigned to the AmIII mode of proteins, was replaced by a narrow and well-defined feature, centered at 1267 cm^{-1} in the 18H spectrum. This band was assigned to a deformation mode of unsaturated acyl chains of lipids, $\delta C=CH$, which is normally expected as a sharp signal at 1260 cm^{-1} (Ishigaki et al. 2019; Heraud et al. 2017; Czamara et al. 2014). Such increment in the content of unsaturated lipid was supported by the change in the shape of the $\nu(C-C)_G$ band (~1070-1095 cm^{-1}), sensitive to the population of methylene groups in *gauche* conformations along the acyl lipid chains (Czamara et al. 2014; Sosa Morales et al. 2015, 2019).

18H spectrum vs 22H spectrum

Drastic differences were observed in the protein-related bands when comparing the representative spectra of the 18H and 22H groups. In the highest wavenumbers region, the prevalence of the band at 2931 cm^{-1} (ν_sCH_3) stood out, which is mainly associated with protein vibrations. In the fingerprint region, several other notorious changes were manifested. Among them, the one experienced by the contour of the composite band with maximum at 1655 cm^{-1}

Table 1 Wavenumbers (cm^{-1}), relative intensities, and tentative assignment of the Raman bands observed in the ~3000–900 cm^{-1} region of the representative-spectra of the four sampling groups generated in this study

0H[a]	6H[a]	18H[a]	22H[a]	Assignment[b]	Reference
2930vs	2930vs	2931vs	2931vs	ν_sCH$_3$ (protein, lipid)	(Heraud et al. 2017; Krafft et al. 2005)
2881vs	2888vs	2888vs	2886vs	ν_{as}CH$_2$ (lipid, protein)	(Czamara et al. 2014; Sosa Morales et al. 2019; Bresson et al. 2006)
2851vs	2851vs	2850vs	2852vs	ν_sCH$_2$ (lipid)	(Heraud et al. 2017; Krafft et al. 2005; Sosa Morales et al. 2015)
1747w	1748w	1747w	1747w	νC=O (phospholipid)	(Heraud et al. 2017; Okotrub et al. 2018; Czamara et al. 2014; Neal 2018)
1732w	1733w	1733w	~1732vw	νC=O (triglyceride)	(Heraud et al. 2017; Okotrub et al. 2018; Czamara et al. 2014; Neal 2018)
1655s/br	1655s	1655s	1655s/br	AmI (protein) // νC=C (lipid)	(Davidson et al. 2013; Jimenez et al. 2019; Rizo et al. 2021; Ishigaki et al. 2019)
~1640sh				AmI (carbohydrate)	(Jimenez et al. 2019; Rizo et al. 2021; Rizo et al. 2016)
1620 m	1620m	1620m	1617m	νTyr	(Heraud et al. 2017; Jimenez et al. 2019; Rizo et al. 2016; Rygula et al. 2013)
1605sh	1602w	1599w	1604sh	νPhe	(Jimenez et al. 2019; Rizo et al. 2021; Rygula et al. 2013; De Gelder et al. 2007)
1441vs	1438vs	1438vs	1442vs	δCH$_3$/CH$_2$ (protein; lipid; carbohydrate)	(Okotrub et al. 2018; Bogliolo et al. 2014; Jimenez et al. 2019; Rizo et al. 2021)
			~1366sh	νTrp	(Rygula et al. 2013; De Gelder et al. 2007; Boyaci et al. 2015)
			1343s	δCC$_\alpha$H (protein)	(Rygula et al. 2013; Boyaci et al. 2015; Jimenez et al. 2019)
1300m	1298s	1297s	1300s	τCH$_2$ (lipid)	(Heraud et al. 2017; Jimenez et al. 2019; Czamara et al. 2014; Petruk et al. 2013)
1265m	1265m	1265s	~1278sh	AmIII (protein) // δC=CH (lipid)	(Jimenez et al. 2019; Rygula et al. 2013; Czamara et al. 2014; Rusciano et al. 2017)
~1258sh	~1258sh		1267m	AmIII (protein)	(Heraud et al. 2017; Jimenez et al. 2019; Ishigaki et al. 2019; Rusciano et al. 2017)
1125m	1125m	1125m	1125m	ν_s(C-C)$_T$ (lipid)	(Davidson et al. 2013; Okotrub et al. 2018; Jimenez et al. 2019; Petruk et al. 2013)
1104w			~1103sh	νC-O / δC-O-H (carbohydrate) // ν_sPO$_2^-$ (phospholipid)	(Heraud et al. 2017; Petruk et al. 2013; Oleinikov et al. 1999; Wu et al. 2011)
1084m	1084m	1083m	1084m	ν(C-C)$_G$ (lipid)	(Sosa Morales et al. 2019; Sosa Morales et al. 2015; Boyaci et al. 2015)
1063w	1063m	1063w	1064w	ν_{as}(C-C)$_T$ (lipid)	(Heraud et al. 2017; Okotrub et al. 2018; Sosa Morales et al. 2019)
1037m	1038sh	1039sh	1037sh	νC-O / δC-O-H (carbohydrate)	(Jimenez et al. 2019; Rizo et al. 2016; De Gelder et al. 2007; Orendorff et al. 2002)
~1027sh	1032w	1032w/br	1032m	νC-C (protein backbone)	(Jimenez et al. 2019; Bogliolo et al. 2013; Kengne-Momo et al. 2012)
1002m	1002w	1001w	1003m	δPhe	(Bogliolo et al. 2012; Rusciano et al. 2017; Rygula et al. 2013)
970w	971m	969m	969w	δC-H (lipid)	(Czamara et al. 2014)
953m	954w	954w	954m	νC-O-C (carbohydrate) // Trp	(Orendorff et al. 2002; Hernández et al. 2013; Kranz et al. 2013; Rygula et al. 2013)
941m	942w	942w	942m	νC-O-C (carbohydrate) // N-Cα-C (protein)	(Krafft et al. 2005; Rygula et al. 2013; Kranz et al. 2013; Hernández et al. 2013)

[a]vs: very strong; s: strong; m: medium; w: weak; vw: very weak; sh: shoulder; br: broad

[b]ν: stretching; δ: deformation; τ: twisting; T: trans; G: *gauche*; s: symmetric; as: antisymmetric; AmI: amide I; AmIII: amide III; Phe: phenylalanine; Tyr: tyrosine; Trp: tryptophan
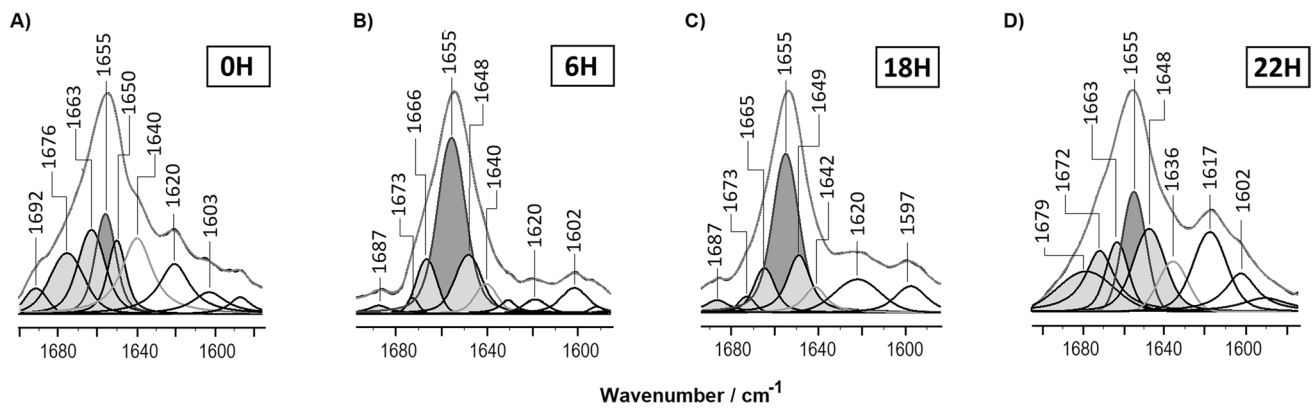
Fig. 4 Decomposition analysis of the four representative-spectra in the 1700-1590 cm^{-1} region. The reconstructed band is superimposed on the original spectrum in order to show the level of fit attained. Component shaded in dark grey (1655 cm^{-1}): ν C=C of unsaturated lipid chains. Components shaded in light grey: protein AmI mode (1692-1687 cm^{-1}, turns; 1676-1673 cm^{-1}, β-sheet, 1663-1666 cm^{-1}, random coil; ~1649 cm^{-1}, α-helix). Component not shaded, grey line (~1640 cm^{-1}): AmI mode of N-acetylated carbohydrates

stood out; it was broader and more irregular in the 22H than in the 18H spectrum (Fig. 3). Upon deconvolution of this band, the AmI components of proteins were found to have gained considerable intensity with respect to the component assigned to νC=C of unsaturated lipids (see Fig. 4 D). In addition, improvement in the bands at 1617 cm^{-1} (νTyr) and 1343 cm^{-1} (δCCαH in protein α-helix structure) was also found.

It is worth mentioning that a single feature at ~1746 cm^{-1} in 22H spectrum (νC=O mode of phospholipids and cholesterols) was observed, while two components were clearly evidenced in the representative spectra of the 0H, 6H, and 18H groups (νC=O mode of triglycerides at 1733 cm^{-1}). This fact suggests that the triglycerides content dropped drastically during the last four hours of the *in vitro* maturation process (Czamara et al. 2014, 2017; Neal 2018). With the exception of this last spectral difference, all the above features indicate that protein abundance prevailed over the other bio-components in oocytes belonging to the 22H group.

Statistical analysis

Interpretations derived from the spectral differences observed between the four representative spectra of bovine oocytes were supported by statistical analyses. Previously, we determined that the peaks at 1300 and 1062 cm^{-1} (τCH$_2$ and ν_{as}(C-C)$_T$ of lipid acyl chains, respectively), 1037 cm^{-1} (νC-O/δC-O-H of carbohydrates), and 1340 and 1003 cm^{-1} (δCCαH and Phe breathing of proteins, respectively) show statistically significant variations between the immature and mature states of bovine oocytes (Jimenez et al. 2019). In the current analysis, the arithmetic means of these variables were re-evaluated by including the intermediate states generated in this study (Fig. 5A).

The lipid vibrations observed at 1300 and 1062 cm^{-1} evidenced a significant enhancement in the 6H spectrum with respect to the control groups (0H) (p= 0.002 and p= 0.0002, respectively) while no statistically significant differences were estimated in the subsequent culturing periods (p> 0.01). Conversely, the mean value of the variable at 1343 cm^{-1} was significantly improved just at the end of the maturation process (p= 0.0001 in the 22H group); the band at 1002 cm^{-1} indicated that in oocytes belonging to the 6H group, the protein content increased approximately 55% (p= 0.006) with respect to the initial maturational state (0H) but rose up to ~130% (p= 0.003) in the 22H group. The opposite trend was manifested by the carbohydrate peak at 1037 cm^{-1}, which progressively decreased in intensity throughout the complete process of IVM, although the magnitude of this change was not statistically significant (p> 0.01).

The subsequent Principal Component Analysis (PCA) yielded two new variables, PC1 and PC2. PC1 scores allowed the drawing of a clear distinction between the oocytes in the 0H and 22H groups: positive values correlated with spectra showing strong contributions both from lipids and proteins and weak ones from carbohydrates, while spectra with high carbohydrate contents yielded a compact cluster of dots with negative PC1 values, as was previously observed from comparison between immature and *in vitro* matured oocytes (Jimenez et al. 2019). The oocytes cultured during intermediate times yielded scores that correlate well with the PC2 variable, according to which samples rich in lipid are positive while those with a high protein content are located in the negative region of the PC2 coordinate (see Fig. 5B).

The ROC analysis allowed additional significant inferences regarding the relative abundances in lipid and proteins that would be sufficient for the oocyte to be competent or

Fig. 5 A Comparison between the arithmetic mean of the peaks specific of lipids (1300 and 1062 cm^{-1}), proteins (1340 and 1002 cm^{-1}), and carbohydrates (1037 cm^{-1}). The peak magnitudes were extracted from the second derivatives calculated for all the average-spectra of the 0H, 6H, 18H, and 22H groups (n=14; 13; 17; 14, respectively). **B** PCA scatter plot (PC1 vs PC2) applied to the 1800-900 cm^{-1} spectral region; each dot represents the average-spectrum of each oocyte
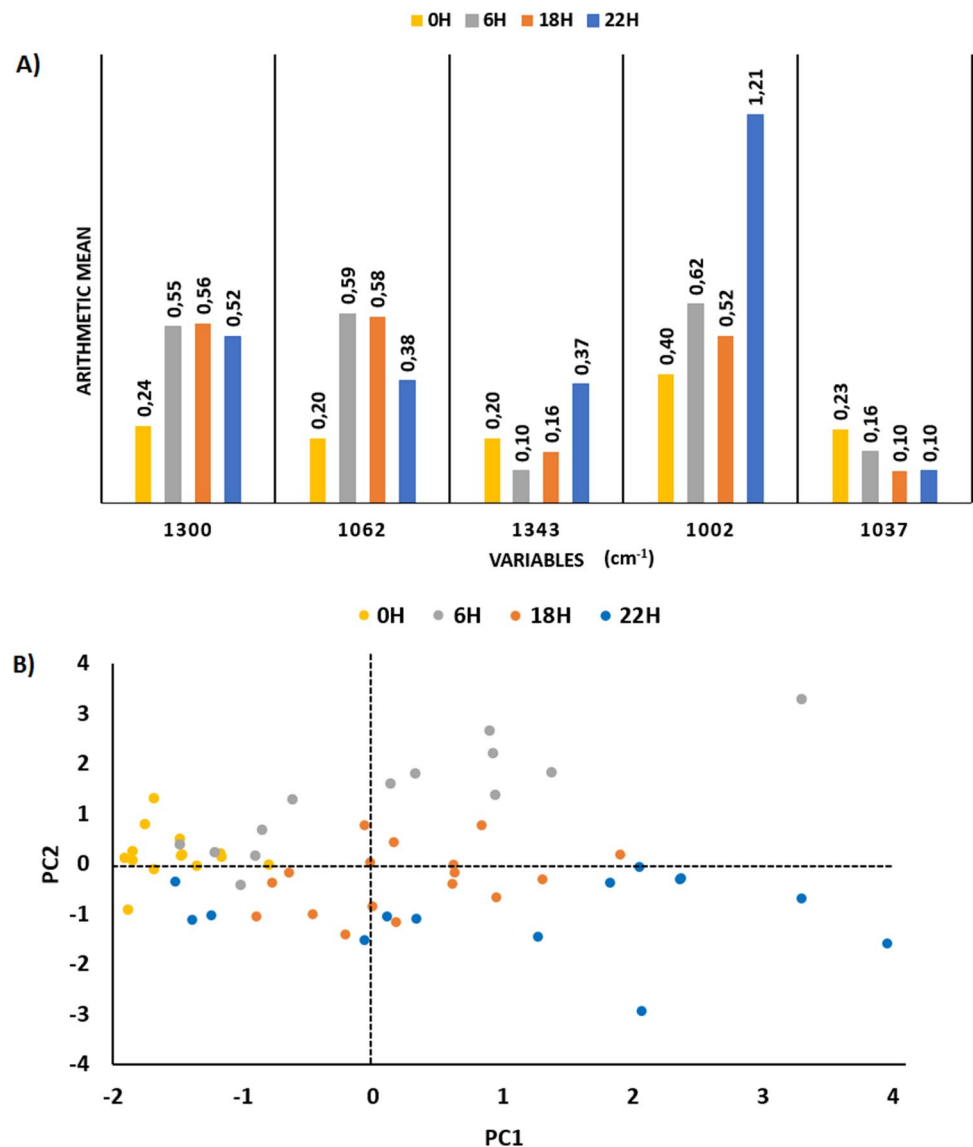

mature enough to successfully carry out subsequent treatments (Davidson et al. 2013). Based on the opposite spectral behavior of carbohydrates regarding those of lipids and proteins, the carbohydrate-to-lipid and carbohydrate-to-protein ratios were estimated by using the intensities (P) of the peaks at 1037, 1300 and 1002 cm^{-1} in the second derivative of each average spectrum. Figure 6 shows the scores corresponding to the P_{1037}/P_{1300} and P_{1037}/P_{1002} ratios calculated for each oocyte; the ratios obtained from the control groups (0H and 22H) yielded the cut-off points, $P_{1037}/P_{1300}= 0.327$ and $P_{1037}/P_{1002}= 0.109$, which provided the reference values to determine the biomarker contents in oocytes belonging to the 6H and 18H groups: scores below the cut-off points corresponded to oocytes with enough lipids or proteins abundances to be considered mature.

The statistical analysis used demonstrated that 77% of the oocytes cultured for 6 hours had a P_{1037}/P_{1300} ratio below

0.327, while this population rose to 88% upon 18 hours of culture. In contrast, the P_{1037}/P_{1002} relationship evidenced that protein accumulation followed a slower and more gradual process since all oocytes cultured for 6 hours hardly showed an increase with respect to the basal content of this bio-component in an immature cytoplasm, whereas 53% of the oocytes cultured for 18 hours were able to cross the cut-off point (Fig. 6B).

Discussion

The present work focuses on the biochemical characterization of the bovine oocyte cytoplasm at two intermediate levels of the maturation process by means of Raman microscopy. In order to track the chronological sequence of the main biochemical changes occurring in the cytoplasm,
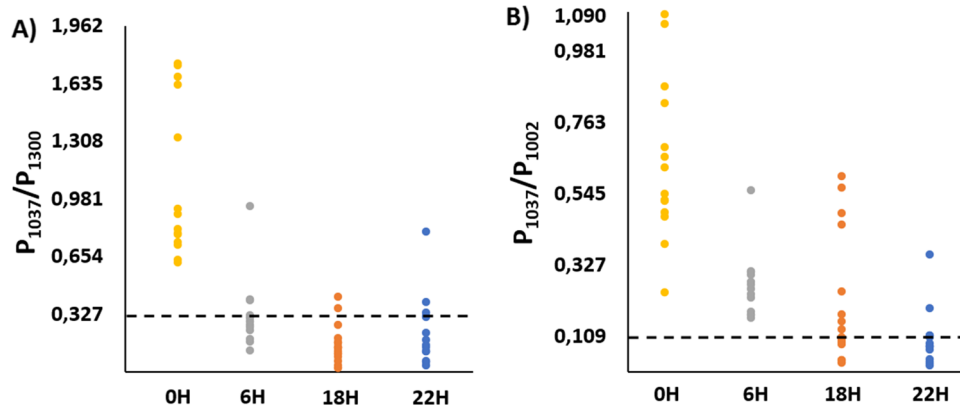
Fig. 6 ROC curves analysis applied to **A** the carbohydrate-to-lipid ratio, P_{1037}/P_{1300}, and **B** the carbohydrate-to-protein ratio, P_{1037}/P_{1002}, both calculated from the second derivative of the average-spectrum of each oocyte of the control groups (0H and 22H) and at intermedi-ate maturation states (6H and 18H). The statistics cut-off points 0.388 and 0.168 constitute the thresholds that determine the global content of lipids and proteins, respectively, necessary for an oocyte to be considered mature

the Raman spectra obtained were compared between them and with those of control groups for immature and *in vitro* matured oocytes. In spite of the complex constitution of the cell, several bands attributed to specific vibrations of lipids, proteins and carbohydrates were identified based on reported data for related biological systems. Statistical analyses performed on a few selected bands associated with exclusive vibrations of the above-mentioned bio-components supported the interpretations derived from the spectra and yielded valuable information concerning their global contents at different maturational status.

The meticulous comparison of spectral profiles was carried out considering two successive maturation times. The starting point of the spectral analysis relied on the previous spectral characterization of the cytoplasm of immature oocytes and of oocytes that completed the maturation time in *vitro* (22 hours), which was conclusive in terms of a marked increase in the lipid and protein contents and the lowered sugar content observed in *in vitro* mature oocytes compared to the immature ones (Jimenez et al. 2019). In concordance, the main spectral differences observed between the 0H and 6H groups evidence a remarkable increase in the lipid content that could be considered the dominant event that occurred during the first six hours of culture. Such increment includes an enhancement in the proportion of unsaturated lipids, which is in line with published results obtained by FT-IR mapping of mouse oocytes that showed a higher content of unsaturated fatty acids in mature oocytes (Wood et al. 2008). The fast increment in this bio-component is justified by the increased number of cytoplasmic organelles, especially mitochondria, rich in phospholipids and mainly located in the periphery at this maturational stage, as well as of cortical granules and lipid droplets, with clustered distribution throughout the cytoplasm (Ferreira et al. 2009; Kruip et al. 1983; Niimura et al. 2004). On the other hand,

the overall intensity decrease in the sugar bands in the 6H representative spectrum can be related to the known glucose metabolic activity which, as reported, is already detectable from the first hour of bovine oocyte culture (Zuelke and Brackettt 1992).

The comparison between the 6H and 18H spectra shows the same trend observed between 0H and 6H in the sense that the lipid content increases as maturation progresses; the C-H stretching bands are forceful as they show the predominance of lipids over proteins (Fig. 2). Nevertheless, the magnitude of the spectral changes in the fingerprint region is less pronounced (Fig. 3). On the other hand, an increase in the cytoplasm protein content is expected during this maturation period, partly due to its participation in the formation of the meiotic spindle (Ferreira et al. 2009; Sirard et al. 1989). However, the slight enhancement observed for several protein bands in the 18H spectrum (e.g., the components assigned to the AmI mode, Fig. 4) were interpreted in terms of a conformational change of the proteins rather than in an increase in the total protein content; the spectral evidence suggests that there were no detectable alterations in the content of this bio-component in the outermost layers of the cytoplasm.

The drastic spectral differences observed between the 18H and 22H groups lead to the conclusion that the main biochemical change during the last stage of the *in vitro* maturation process consists in the sharp increase in protein content. Its final abundance could even exceed the content of lipids, based on the relative intensities of specific bands such as those at 1343 and 1003 cm^{-1}, which became stronger than the lipid signals at 1265 cm^{-1} (δC=CH) and between 1125-1064 cm^{-1} (νC=C of acyl chains), see Table 1. On the other hand, the inferred decrease in the proportion of triglycerides from the almost disappearance of the signal at 1733 cm^{-1} is consistent with the role of this bio-component as an energy

source in ATP synthesis, necessary for protein production and other biological processes (Kruip et al. 1983), and is in agreement with previous studies that demonstrated lower triglycerides content in *in vitro* matured bovine oocytes than in immature ones (Ferguson and Leese 1999, 2006; Kim et al. 2001; McEvoy et al. 2000).

The main events that constitute the cytoplasmic maturation process, synthetically described as redistribution of cytoplasmic organelles, dynamics of the cytoskeletal filaments and molecular maturation (Ferreira et al. 2009), were demonstrated to be concisely manifested in the Raman spectra through abrupt intensifications of signals specific of lipids and proteins that occurred at the early and final stages, respectively, of the maturation process. In addition, a progressive decrease in the carbohydrate bands was observed from the 6H spectrum onwards.

Statistical analysis supported spectral observations and provided additional interpretations from the behavior of specific vibration bands. Principal Component Analysis confirmed that almost all the oocytes belonging to the 6H group showed a marked dominancy of lipid contribution, whereas those in the 18H group showed larger variability in the three main bio-components. Oocytes belonging to the 22H group were well-characterized by the high lipids and proteins and low carbohydrates contents; the location of a few dots (22%) belonging to the 22H group at the negative region of the PC1 variable was consistent with the known fact that the *in vitro* maturation method is not totally reliable (Jimenez et al. 2019; Rizo et al. 2016; Roldán-Olarte et al. 2017). Indeed, the analyses of the nuclear maturation by epifluorescence microscopy assays indicated that approximately 74% of the oocytes reach the MII stage at 22 hours of IVM. PCA analyses also allowed concluding that the process of accumulation of proteins in the cytoplasm develops in a more gradual way than the increase in lipids, since only at 18 hours of culture did 50% of the oocytes reach the adequate protein content to be considered mature. In turn, the ROC curve analysis revealed that approximately 77% of the oocytes cultured for six hours exceeded the threshold indicative of the minimum lipid content in mature oocytes. However, since the evaluation by nuclear staining of the 6H group evidenced that 100% of the oocytes remained in the GV stage, we concluded that the lipid bands are not suitable parameters to assess the maturational state of the oocyte. Conversely, the protein content estimation derived from the spectral data and the subsequent multivariate analysis are in fairly good concordance with the results here obtained by the evaluation of the nuclear maturation state as well as with those previously acquired by other approaches (Rizo et al. 2016; Giotto et al. 2015; Roldán-Olarte et al. 2017; Rahim et al. 2011; B. Wu et al. 1999). In this way, the protein content was verified to be essential for the determination of the maturation state of the oocyte, in agreement with what was proposed by Davidson et al. (2013). Finally, the carbohydrate-to-protein (P_{1037}/P_{1002}) ratio proved to be sensitive enough to determine the cytoplasmic maturation state of bovine oocytes and promises to be useful in future research aimed at optimizing culture conditions through the promotion of protein accumulation in the ooplasm.

Conclusions

The Raman spectral analysis of the cytoplasm of bovine oocytes at two intermediate levels of the maturation process is presented and compared with control groups for immature and *in vitro* matured oocytes in order to track the chronological sequence of the main biochemical changes occurring along the process. Statistical analyses performed on a few selected bands associated with exclusive vibrations of proteins, lipids or carbohydrates supported the interpretations derived from the spectra and yielded valuable information concerning the global contents of these bio-components at different maturational status. Specifically, the features at 1300, 1002, and 1037 cm^{-1} demonstrated statistically significant differences throughout the maturation process.

This work proves that Raman microscopy is a useful diagnostic tool for the adequate evaluation of the maturation state of the oocyte and lays the foundations for future studies focused on the search for optimal culture media by monitoring the evolution of global lipid and protein contents in the cytoplasm of oocytes subjected to *in vitro* maturation.

Authors' contributions LEJ: Performed research, analyzed data and wrote the paper; ACJ: Analyzed data; MRO: Conceived study and performed research; RMSA: Conceived study, performed research and wrote the paper. All authors read and approved the final article.

Data availability Data are available from the corresponding author upon request.

Code availability Not applicable.

Declarations

Ethics approval Not applicable. Samples were provided by a certified local abattoir.

Consent for publication Not applicable.

References

Bogliolo L, Ledda S, Innocenzi P, Ariu F, Bebbere D, Rosati I, Giuseppe G, Piccinini M (2012) Raman microspectroscopy as a non-invasive tool to assess the vitrification-induced changes of ovine oocyte zona pellucida. Cryobiology 64:267–272. https://doi.org/10.1016/j.cryobiol.2012.02.010

Bogliolo L, Leoni GG, Ledda S (2020) Raman spectroscopy-based approach to study the female gamete. Theriogenology 150:268–275. https://doi.org/10.1016/j.theriogenology.2020.01.059

Bogliolo L, Murrone O, Di Emidio G, Piccinini M, Ariu F, Ledda S, Tatone C (2013) Raman spectroscopy-based approach to detect aging-related oxidative damage in the mouse oocyte. J Assist Reprod Genet 30:877–882. https://doi.org/10.1007/s10815-013-0046-6

Bogliolo L, Murrone O, Piccinini M, Ariu F, Ledda S, Tilocca S, Albertini DF (2014) Evaluation of the impact of vitrification on the actin cytoskeleton of in vitro matured ovine oocytes by means of raman microspectroscopy. J Assist Reprod Genet 32:185–193. https://doi.org/10.1007/s10815-014-0389-7

Bonnier F, Byrne HJ (2012) Understanding the molecular information contained in principal component analysis of vibrational spectra of biological systems. Analyst 137:322–332. https://doi.org/10.1039/C1AN15821J

Boyaci IH, Temiz HT, Geniş HE, Soykut EA, Yazgan NN, Güven B, Uysal RS, Bozkurt AG, İlaslan K, Torun O, Şeker FCD (2015) Dispersive and FT-Raman spectroscopic methods in food analysis. RSC Adv 5:56606–56624. https://doi.org/10.1039/C4RA12463D

Bresson S, El Marssi M, Khelifa B (2006) Conformational influences of the polymorphic forms on the C o and C –H stretching modes of five saturated monoacid triglycerides studied by Raman spectroscopy at various temperatures. Vib Spectrosc 40:263–269. https://doi.org/10.1016/j.vibspec.2005.11.001

Czamara K, Majzner K, Pacia MZ, Kochan K, Kaczor A, Baranska M (2014) Raman spectroscopy of lipids: a review. J Raman Spectrosc 46:4–20. https://doi.org/10.1002/jrs.4607

Czamara K, Majzner K, Selmi A, Baranska M, Ozaki Y, Kaczor A (2017) Unsaturated lipid bodies as a hallmark of inflammation studied by Raman 2D and 3D microscopy. Sci Rep 7:1–10. https://doi.org/10.1038/srep40889

Davidson B, Murray AA, Elfick A, Spears N (2013) Raman microspectroscopy can be used to investigate the developmental stage of the mouse oocyte. PLoS ONE 8:e67972–e67981. https://doi.org/10.1371/journal.pone.0067972

De Gelder JD, Gussem KD, Vandenabeele P, Moens L (2007) Reference database of Raman spectra of biological molecules. J Raman Spectrosc 38:1133–1147. https://doi.org/10.1002/jrs.1734

Ferguson EM, Leese HJ (1999) Triglyceride content of bovine oocytes and early embryos. J Reprod Fertil 116:373–378. https://doi.org/10.1530/jrf.0.1160373

Ferguson EM, Leese HJ (2006) A potential role for triglyceride as an energy source during bovine oocyte maturation and early embryo development. Mol Reprod Dev 73:1195–1201. https://doi.org/10.1002/mrd.20494

Ferreira EM, Vireque AA, Adona PR, Meirelles FV, Ferriani RA, Navarro PAAS (2009) Cytoplasmic maturation of bovine oocytes: structural and biochemical modifications and acquisition of developmental competence. Theriogenology 71:836–848. https://doi.org/10.1016/j.theriogenology.2008.10.023

García DC, Miceli DC, Rizo G, García EV, Valdecantos PA, Roldán-Olarte M (2015a) Expression and localization of urokinase-type plasminogen activator receptor in bovine cumulus–oocyte complexes. Zygote 24:230–235. https://doi.org/10.1017/S0967199415000076

García EV, Miceli DC, Rizo G, Valdecantos PA, Barrera AD (2015b) Effect of early addition of bone morphogenetic protein 5 (BMP5) to embryo culture medium on in vitro development and expression of developmentally important genes in bovine preimplantation embryos. Theriogenology 5:589–599. https://doi.org/10.1016/j.theriogenology.2015.04.018

Giotto AB, Dos Santos BD, Francielli WS, Guimarães ACG, Gonçalves CGM, Pavin CUM, Folchini NP, Moyses AB, Missio D, Leivas FG (2015) Oxygen tension and oocyte density during in vitro maturation affect the in vitro fertilization of bovine oocytes. Semina: Ciências Agrárias 36(4277–88). https://doi.org/10.5433/1679-0359.2015v36n6Supl2p4277

Heraud P, Marzec KM, Zhang QH, Yuen WS (2017) Label-free in vivo Raman microspectroscopic imaging of the macromolecular architecture of oocytes. Sci Rep 7:31–34. https://doi.org/10.1038/s41598-017-08973-0

Hernández B, Pflüge F, Kruglik SG, Ghomi M (2013) Characteristic Raman lines of phenylalanine analyzed by a multiconformational approach. J Raman Spectrosc 44:827–833. https://doi.org/10.1002/jrs.4290

Ishigaki M, Hoshino Y, Ozaki Y (2019) Phosphoric acid and phosphorylation levels are potential biomarkers indicating developmental competence of matured oocytes. Analyst 144:1527–1534. https://doi.org/10.1039/C8AN01589A

Jimenez LE, Roldán-Olarte M, Álvarez MRS (2019) Raman microscopy analysis of the biochemical changes in the cytoplasm of bovine oocytes induced by an in vitro maturation process: interference of the zona pellucida. ChemistrySelect 4:3706–3716. https://doi.org/10.1002/slct.201803454

Kengne-Momo RP, Daniel Ph, Lagarde F, Jeyachandran YL, Pilard JF, Durand-Thouand JM, Thouand G (2012) Protein interactions investigated by the Raman spectroscopy for biosensor applications. Int J Spectrosc 2012:1-7. https://doi.org/10.1155/2012/462901

Kim JY, Kinoshita M, Ohnishi M, Fukui Y (2001) Lipid and fatty acid analysis of fresh and frozen – thawed immature and in vitro matured bovine oocytes. Reproduction 122:131–138. https://doi.org/10.1530/rep.0.1220131

Krafft C, Knetschke T, Funk RHW, Salzer R (2005) Identification of organelles and vesicles in single cells by Raman microspectroscopic mapping. Vib Spectrosc 38:85–93. https://doi.org/10.1016/j.vibspec.2005.02.008

Kranz J, AlAzzam F, Saluja A, Svitel J, Al-Azzam W (2013) Techniques for higher-order structure determination. In: Narhi LO (ed) Biophysics for Therapeutic Protein Development. Biophysics for the Life Sciences 4. 1st edn. Springer, New York, pp 33-82.

Kruip TAM, Cran DG, Van Beneden TH, Dieleman SJ (1983) Structural changes in bovine oocytes during final maturation in vivo. Gamete Res 47:29–47. https://doi.org/10.1002/mrd.1120080105

Lee C, Bain CD (2005) Raman spectra of planar supported lipid bilayers. Biochim Biophys Acta 1711:59–71. https://doi.org/10.1016/j.bbamem.2005.02.006

Lonergan P, Fair T (2016) Maturation of oocytes in vitro. Annu Rev Anim Biosci 4:255–268. https://doi.org/10.1146/annurev-animal-022114-110822

Marquardt DW (1963) An algorithm for least-squares estimation of nonlinear parameters. SIAM J Appl Math 11:431–441. https://doi.org/10.1137/0111030

McEvoy TG, Coull GD, Broadbent PJ, Hutchinson JSM, Speake BK (2000) Fatty acid composition of lipids in immature cattle, pig

and sheep oocytes with intact zona pellucida. J Reprod Fertil 118:163–170. https://doi.org/10.1530/jrf.0.1180163

Neal SL (2018) Multivariate analysis of mixed lipid aggregate phase transitions monitored using Raman pectroscopy. Appl Spectrosc 72:102–113. https://doi.org/10.1364/AS.72.000102

Niimura S, Kawakami S, Takano H (2004) Changes in the amount of cytoplasmic inclusions in mouse oocytes during meiotic maturation in vivo and in vitro. Reprod Med Biol 3:231–236. https://doi.org/10.1111/j.1447-0578.2004.00075.x

Niimura S, Takano H, Onishi A, Hosoe M (2002) Changes in the amount of proteins, glycogen and lipids in porcine oocytes during in vitro meiotic maturation. J Anim Sci 73:327–332. https://doi.org/10.1046/j.1344-3941.2002.00045.x

Okotrub KA, Mokrousova VI, Amstislavsky SY, Surovtsev NV (2018) Lipid droplet phase transition in freezing cat embryos and oocytes probed by Raman spectroscopy. Biophys J 115:1–11. https://doi.org/10.1016/j.bpj.2018.06.019

Oleinikov VA., Kovner MA, Ermishov MA, Tuzikov AB, Bovin NV, Nabiev IR (1999) Raman spectroscopy of sialic acids. Spectral bands of a-(2~3)- and a-(2~6)- sialyllinkages of oligosaccharides. In: Greve J et al. (eds) Spectroscopy of Biological Molecules: New Directions. Kluwer Academic Publishers, pp 331–332. doi: https://doi.org/10.1007/978-94-011-4479-7_148

Orendorff CJ, Ducey MW, Pemberton JE (2002) Quantitative correlation of Raman spectral indicators in determining conformational order in alkyl chains. J Phys Chem A 106:6991–6998. https://doi.org/10.1021/jp014311n

Petruk AA, Álvarez MRS (2013) Structural Changes Induced by Interactions between Thyroid Hormones and Phospholipid Membranes: A Raman Spectroscopy Study. J Raman Spectrosc 44:346–354. https://doi.org/10.1002/jrs.4205

Petruk AA, Sosa Morales MC, Álvarez MRS (2013) Iodothyronine – phospholipid interactions in the lipid gel phase probed by Raman spectral markers. Spectrochim Acta A Mol Biomol Spectrosc 112:403–409. https://doi.org/10.1016/j.saa.2013.04.094

Rahim B, Jalal S, Yosef N (2011) Effect of cysteine supplementation on in vitro maturation of bovine oocyte. Afr J Biotechnol 10:15830–15833. https://doi.org/10.5897/AJB11.1686

Rizo G, Barrera AD, Jimenez LE, García EV, García DC, Roldán-Olarte M (2021) Exogenous activation and inhibition of plasminogen / plasmin activity during in vitro maturation of bovine cumulus - oocyte complexes: a biological and spectroscopic approach. Mol Reprod Dev 88:1–13. https://doi.org/10.1002/mrd.23441

Rizo G, Roldán-Olarte M, Miceli DC, Jimenez LE, Álvarez MRS (2016) Structural modifications induced by an in vitro maturation process in zona pellucida glycoproteins. RSC Adv 6:83429–83437. https://doi.org/10.1039/C6RA06243A

Rizos D, Ward F, Duffy P, Boland MP, Lonergan P (2002) Consequences of bovine oocyte maturation, fertilization or early embryo development in vitro versus in vivo: implications for blastocyst yield and blastocyst quality. Mol Reprod Dev 61:234–248. https://doi.org/10.1002/mrd.1153

Roldán-Olarte M, Maillo V, Sánchez-Calabuig JM, Beltrán-Breña P, Rizos D, Gutiérrez-Adán A (2017) Effect of urokinase type plasminogen activator on in vitro bovine oocyte maturation. Reproduction 154:231–240. https://doi.org/10.1530/REP-17-0204

Rusciano G, De Canditiis C, Zito G, Rubessa M, Roca S, Carotenuto R, Sasso A, Gasparrini B (2017) Raman-microscopy investigation of vitrification-induced structural damages in mature bovine oocytes. PLoS ONE 1–19. doi: https://doi.org/10.1371/journal.pone.0177677

Rygula A, Majzner K, Marzec KM, Kaczor A, Pilarczyk M, Baranska M (2013) Raman spectroscopy of proteins: a review. J Raman Spectrosc 44:1061–1076. https://doi.org/10.1002/jrs.4335

Savitzky A, Golay MJE (1964) Smoothing and differentiation of data by simplified least squares procedures. Anal Chem 36:1627–1639. https://doi.org/10.1021/ac60214a047

Sirard MA, Florman HM, Leibfried-Rutledge ML, Barnes FL, Sims ML, First NL (1989) Timing of nuclear progression and protein necessary for meiotic maturation of bovine synthesis. Biol Reprod 40:1257–1263. https://doi.org/10.1095/biolreprod40.6.1257

Sosa Morales MC, Juárez AC, Álvarez MRS (2015) Raman spectroscopy study of the interaction of phosphatidylglycerol lipid bilayers. J Raman Spectrosc 46:302–308. https://doi.org/10.1002/jrs.4639

Sosa Morales MC, Juárez AC, Montich GG, Álvarez MRS (2019) interaction of the antibiotic peptide nisin with anionic membranes in different phase-states: a vibrational study. Spectrochim Acta A Mol Biomol Spectrosc 215:389–97. doi: https://doi.org/10.1016/j.saa.2019.03.009; https://doi.org/10.1366/0003702884428905

Ward F, Enright B, Rizos D, Boland M, Lonergan P (2002) Optimization of in vitro bovine embryo production: effect of duration of maturation, length of gamete co-incubation, sperm concentration and sire. Theriogenology 57:2105–2017. https://doi.org/10.1016/S0093-691X(02)00696-9

Wood BR, Chernenko T, Mattha C, Diem M, Chong C, Bernhard U, Jene C, Brandli AA, McNaughton D, Tobin MJ, Trounson A, Lacham-Kaplan O (2008) Shedding new light on the molecular architecture of oocytes using a combination of synchrotron Fourier Transform-Infrared and Raman spectroscopic mapping. Anal Chem 80:9065–9072. https://doi.org/10.1021/ac8015483

Wu B, Tong J, Leibo SP (1999) Effects of cooling germinal vesicle – stage bovine oocytes on meiotic spindle formation following in vitro maturation. Mol Reprod Dev 54:388–395. doi: https://doi.org/10.1002/(SICI)1098-2795(199912)54:4%3C388::AID-MRD9%3E3.0.CO;2-7

Wu H, Volponi JV, Oliver AE, Parikh AN, Simmons BA, Singh S (2011) In vivo lipidomics using single-cell Raman spectroscopy. PNAS 108:3809–3814. https://doi.org/10.1073/pnas.1009043108

Zuelke KA, Brackettt BG (1992) Effects of luteinizing in cumulus-enclosed on glucose metabolism bovine oocytes matured in vitro. Endocrinology 131:2690–2696. https://doi.org/10.1210/endo.131.6.1446610